ELSEVIER

Land cover-based optimal deconvolution of PALS L-band microwave brightness temperatures

Ashutosh S. Limaye[a],*, William L. Crosson[a], Charles A. Laymon[a], Eni G. Njoku[b]

[a] Global Hydrology and Climate Center, NSSTC, Universities Space Research Association, 320 Sparkman Dr., Huntsville, AL 35805, USA
[b] Jet Propulsion Laboratory, M/S 300-233, 4800 Oak Grove Dr., Pasadena, CA 91109, USA

Abstract

An optimal deconvolution (ODC) technique has been developed to estimate microwave brightness temperatures of agricultural fields using microwave radiometer observations. The technique is applied to airborne measurements taken by the Passive and Active L and S band (PALS) sensor in Iowa during Soil Moisture Experiments in 2002 (SMEX02). Agricultural fields in the study area were predominantly soybeans and corn. The brightness temperatures of corn and soybeans were observed to be significantly different because of large differences in vegetation biomass. PALS observations have significant over-sampling; observations were made about 100 m apart and the sensor footprint extends to about 400 m. Conventionally, observations of this type are averaged to produce smooth spatial data fields of brightness temperatures. However, the conventional approach is in contrast to reality in which the brightness temperatures are in fact strongly dependent on land cover, which is characterized by sharp boundaries. In this study, we mathematically deconvolve the observations into brightness temperature at the field scale (500–800 m) using the sensor antenna response function. The result is more accurate spatial representation of field-scale brightness temperatures, which may in turn lead to more accurate soil moisture retrieval.
© 2004 Elsevier Inc. All rights reserved.

1. Introduction

Microwave brightness temperatures (TB) have been used effectively for soil moisture retrieval (Engman & Chauhan, 1995; Jackson, 1993; Jackson et al., 1999, 1995, 1997b, 1997a; Jackson & Schmugge, 1989; Laymon et al., 1999, 2001). Several airborne sensors have been used for measuring received energy in various wavelengths including L (~ 1.4 GHz), S (~ 2.5 GHz) and C (~ 7 GHz) bands. Typically, the instantaneous field of view (IFOV) of these sensors is significantly greater than the spacing between adjacent footprints, i.e. the target surface is over-sampled. Creating gridded data on spatial scales finer than the IFOV from the sensor observations results in significant smoothing. In this study, a technique is developed that exploits the over-sampling to provide accurate field-scale estimates of TB that exhibit heterogeneity and distinct boundaries consistent with the landscape. The brightness temperatures

estimated from this technique will subsequently allow more accurate retrieval of field-scale soil moisture.

The analysis presented here is based on data collected during Soil Moisture Experiments in 2002 (SMEX02) conducted in the summer of 2002 around Ames, IA (Cosh et al., 2004 this issue; http://hydrolab.arsusda.gov/smex02/). Ground sampling teams made daily measurements of soil moisture and temperature and periodic measurements of vegetation parameters at selected predetermined sites. The experiment was conducted with the principle goal of validating brightness temperatures and soil moisture retrieval algorithms using data from the Advanced Microwave Scanning Radiometer for the Earth Observing System (AMSR-E) launched in May 2002. In support of this effort, several passive and active microwave instruments on aircraft were deployed to measure microwave emissions at higher resolution. One such sensor was the Passive and Active L and S band (PALS) microwave instrument, a dual polarization sensor flown over the watershed study area (Wilson et al., 2001). Analysis of individual PALS measurements reveals gradual smoothing of observed values in adjacent observations. When overlaid with the land cover

* Corresponding author. Tel.: +1-256-961-7903; fax: +1-256-961-7304.
E-mail address: Ashutosh.Limaye@msfc.nasa.gov (A.S. Limaye).

classification, the transitions in PALS brightness temperature between soybean and corn are seen to be gradual, in contrast to the almost binary SMEX02 landscape. Corn and soybean vegetation water content were significantly different during the study period. The average vegetation water content for corn was approximately 4 kg/m^2, whereas the average for soybeans was 0.5 kg/m^2. Vegetation water content variability within the same crop type was much smaller than the between-crop type differences (Anderson et al., 2004 this issue). Therefore, the corn or soybean within-field TB variability is expected to be much lower than the between-field variability. Smoothing occurs due to the sensor antenna response function, since each observation covers more than one field and adjacent observations have varying contributions from those land cover types. Conventional interpolation techniques rely on the value of adjacent observations as the basis for interpolation. The two most commonly used interpolation techniques, inverse distance weighted interpolation (IDW) and Kriging (Maidment, 1993), produce comparable interpolation results for PALS observations; IDW is used in this analysis to represent the conventionally interpolated TB. IDW interpolation is simply two-dimensional linear interpolation in which the weights applied to each observation are inversely related to the distance from the point at which the interpolated value is being calculated. Use of these interpolation schemes without correcting for the antenna pattern results in a smooth brightness temperature field with suppressed between-field variability, in contrast to reality in which the brightness temperatures have sharp boundaries at the intersection of fields of different vegetation types. This was the motivation for exploring a different approach to improve the mapping and gridding of airborne microwave brightness temperature observations. Our approach is to impose the sensor antenna response function on the land surface and to extract individual land cover contributions to every observation, thereby mapping TB at the scale of the agricultural fields and preserving the strong between-field variability. This approach has some similarities to those described by Long and Daum (1998) and Poe (1990), but is developed here for specific application to situation in which the spatial boundaries of contributing emitting sources are known a priori. This application requires over-sampling whereby the mean distance between the microwave observations is shorter than the length of the typical agricultural field, so that on average there are multiple observations per field.

2. Study area and data

2.1. Study area

The Walnut Creek study area overflown by PALS was approximately 300 km^2. During the first half of the experiment (10 days), soils in the study area were dry (volumetric water content 8–10%). Variable rainfall amounts in the study area on July 5–6 increased the moisture content to 15–25%. Daily soil moisture measurements were made at selected locations throughout the study area. Vegetation properties were also measured at different times during the experiment at those locations. In this analysis, data from July 2 are used to represent dry conditions, whereas data from July 7 are used for wet conditions. Results for July 7 are emphasized because it followed scattered rainfall in the study area, resulting in high spatial variability of soil moisture.

2.2. PALS data

The PALS microwave instrument is a recent contribution to the inventory of aircraft-based instruments. The passive instrument operates at L band (1.41-GHz radiometer) and S band (2.69-GHz radiometer) with dual polarization and an incidence angle of 45°. Data from the passive L band horizontal polarization are used in this paper. The instrument is flown on a C-130 aircraft, with the antennas viewing out the rear door directed downwards and to the rear of the aircraft. The instrument is non-scanning, thus a single-footprint track is sampled along the flight path. During SMEX02, PALS data were collected along 11 flight lines in the Walnut Creek region south of Ames, IA on 8 days between June 25 and July 8, 2002. The flying altitude of the aircraft was 1162 m, with variations limited to just a few meters for all of the observations on all days. The PALS brightness temperature observations were spaced about 100 m apart (after calibration preprocessing). The footprint of each observation was elliptical, measuring about 350 m across track and 450 m along track (for L-band) at half power beam width.

2.3. Land cover classification

Land cover characterization was performed using Landsat Enhanced Thematic Mapper scenes from May 14, July 1 and July 17, 2002. A tassel cap transformation was performed on the July 1 image and a standard NDVI with red and near-infrared bands was computed using the May 14 and July 17 images. The three output bands of the tassel cap transformation and the two NDVI images were used to partition the land surface into objects based on spatially contiguous spectral characteristics. The objects are referred to as 'segments' based on scale and similarity criteria defined by the image analyst. For this investigation, segments were defined to represent agricultural fields. The typical corn or soybean field dimension is 500–800 m. Subsequently, the segments were classified using the tassel cap transformation and two NDVI images with equal weight in a supervised classification with 11 classes, with the two dominant classes, corn and soybeans, constituting over 80% of the area covered by PALS observations. The classification was verified to be 100% accurate at 31 study sites in the PALS mapping area.

3. Optimal deconvolution method

The optimal deconvolution (ODC) method consists of three steps. The first step is to approximate the sensor antenna response function on the plane normal to the beam axis. The second step is to project this function onto the horizontal (Earth) surface and to calculate the volume under this surface for each land cover segment within the sensor footprint. Finally, a solution of an overdetermined system of equations is found by minimizing the mean absolute difference between ODC-estimated and observed brightness temperatures. Details of the technique are provided in the following sections.

3.1. Sensor antenna response function over the land cover segments

The basic assumption of this technique is that sensor-observed brightness temperatures (or 'antenna temperatures') are linear combinations of the contributing land cover segments, expressed as a two-dimensional spatial convolution of the sensor antenna response function with the actual brightness temperature distribution (Ulaby et al., 1986). The emitted energy contributions of each segment are therefore not treated as uniform, but rather as functions of the sensor antenna response function and the proportion of the segment that is within the footprint. Under the approximation (for simplicity) that the antenna response function can be reasonably well represented by a Gaussian surface, the volume

under the surface covering each segment can be integrated to estimate the true contribution of that segment to the overall sensor observation.

The PALS S-band antenna response function is given by Wilson et al. (2001). S-band half power beam width (3 dB beam width, from which approximately 50% of the power is received) is approximately $13°$. Since the L- and S-band instrument antennas are scaled versions of one another, L-band half power beam width can be approximated to $12°$ (based on L-band wavelength of 21.3 cm and aperture diameter 100 cm, 3-dB beam width in radians for the L-band conical horn can be approximated by the ratio of wavelength and aperture diameter). A Gaussian function can be used as a reasonable approximation to the shape of the response function close to the beam axis. Because PALS has an incidence angle of $45°$, each point on the horizontal surface must be projected onto the beam-normal plane. Fig. 1 illustrates the projection of the Gaussian function from the beam-normal plane to the assumed horizontal Earth surface. The Gaussian surface has radial symmetry on the beam-normal plane; therefore, the power received at the sensor ($P(r)$) from any point at a radial distance r from the beam axis on the beam-normal plane is given by:

$$P(r) = \frac{1}{\sigma\sqrt{2\pi}} e^{\frac{-r^2}{2\sigma^2}} \tag{1}$$

The Gaussian function has only one parameter, the variance (σ^2). From the beam width and sensor altitude, r
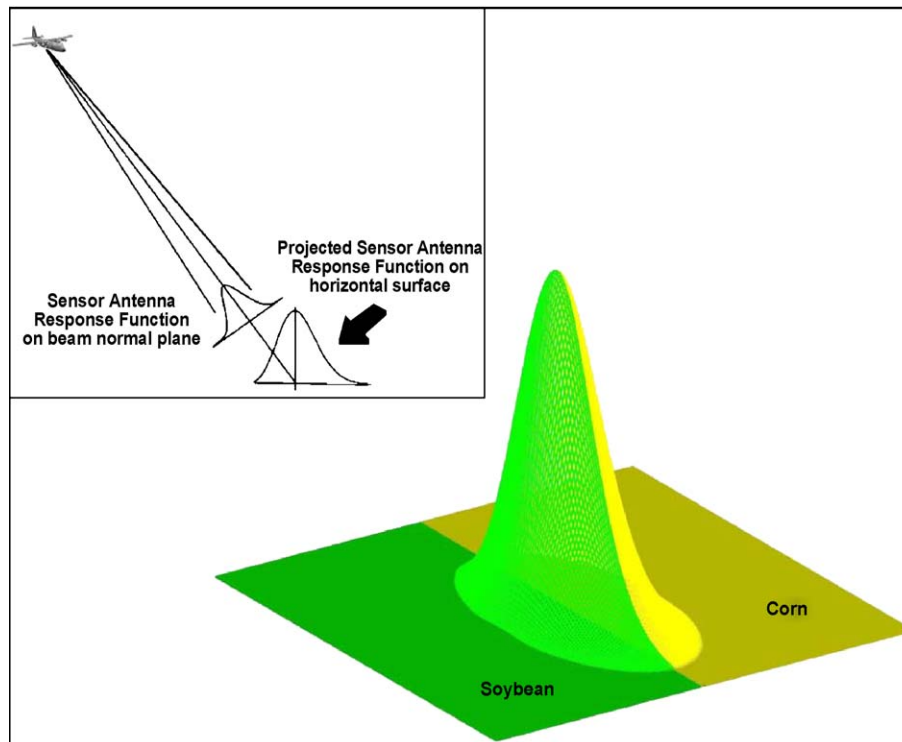

Fig. 1. Illustration of the projection of the antenna response function onto the horizontal Earth surface.

can be computed for any point on the beam-normal plane and Eq. (1) can be solved for σ^2.

Defining the origin of our 3-D space as the point where the beam axis intersects the horizontal (Earth) surface, the sensor location becomes $(X_s, 0, H)$ where

$$X_s = H\tan\phi \tag{2}$$

where H is the altitude of the sensor and ϕ is the sensor incidence angle. The equation for the plane through the origin and normal to the beam is given by:

$$X_sX + HZ = 0 \tag{3}$$

Substitution from Eq. (2) yields:

$$X\tan\phi + z = 0 \tag{4}$$

Any arbitrary point $(X_1, Y_1, 0)$ on the horizontal surface can be projected onto the beam-normal plane at (X_p, Y_p, Z_p) by solving the system of equations defined by Eq. (4) and the parametric representation of the vector from the sensor location $(X_s, 0, H)$ to the arbitrary point $(X_1, Y_1, 0)$. This yields the following solution:

$$X_p = \frac{HX_1}{H + (X_s - X_1)\tan\phi} \tag{5}$$

$$Y_p = Y_1\left[1 + \frac{X_1\tan\phi}{H + (X_s - X_1)\tan\phi}\right] \tag{6}$$

$$Z_p = \frac{-HX_1\tan\phi}{H + (X_s - X_1)\tan\phi} \tag{7}$$

The distance r of any point (X_p, Y_p, Z_p) on the beam-normal plane to the origin is then given by:

$$r = \sqrt{X_p^2 + Y_p^2 + Z_p^2} \tag{8}$$

To compute the total volume under the Gaussian surface, the irregular land cover segments in the sensor field of view are discretized over a fine (10 m) resolution grid on the horizontal plane with the center of the beam as the origin (Fig. 1). The corners of each grid cell are projected to the beam-normal plane using Eqs. (5)–(8), and the areas of all cells on the beam-normal plane are computed. The Gaussian function (Eq. (1)) gives the weights for each cell on the beam-normal plane. These weights are normalized with the corresponding beam-normal cell areas since those on the beam-normal plane are not constant, even though the corresponding cells on the horizontal plane are of equal area. The extent of the 10 m grid is defined so as to cover 90% of the sensor power returned. At the PALS altitude of 1162 m and incidence angle of 45°, the grid on the horizontal plane extends to approximately 350 m radius in the beam-normal plane, resulting in an ellipse of along-track radius of 520 m and across-track radius of 350 m.

3.2. Determining an optimal solution

In order to co-locate the land cover segments and PALS observations, each is mapped to the same fine resolution grid. These PALS observations are referred to here as 'postings'. Even though each posting is associated with a point on the ground where the beam intersects the surface, it is important to note that each posting represents the observation made by the sensor within its field of view. All the cell weights within a segment are integrated to determine the segment's fractional contribution to the individual posting. These segment-fractional contributions, normalized over all the integrals within the field of view, give what is termed as a segment Gaussian fraction (ranging from 0 to 1). Over-sampling in the observations allow several PALS postings to cover the same land cover segments, but with varying Gaussian fractions. Therefore, we can deconvolve the observed sensor brightness temperatures into segment brightness temperatures by simultaneously solving the neighboring PALS postings with the corresponding contributions from the land cover segments. The synthesized or ODC-reconstructed sensor brightness temperatures are calculated as the summation of all brightness temperatures from contributing segments multiplied by their respective Gaussian fractions. Because there are more equations (number of postings) than unknowns (segment TB), there is no unique solution. Therefore, an "optimal" solution is defined to minimize the difference between the ODC-reconstructed brightness temperatures and the postings. The optimization problem is defined by the objective function:

$$\text{Minimize} \sum^{\text{All PALS postings}} |\text{ODC reconstructed posting TB} - \text{observed posting TB}| \tag{9}$$

where:

$$\text{ODC reconstructed posting TB} = \sum^{\text{All underlying land cover segments}} (\text{Gaussian fraction}) \times (\text{segment TB}) \tag{10}$$

4. Results

4.1. Comparison of PALS observed brightness temperatures with ODC-reconstructed postings

The accuracy of the optimization algorithm can be easily demonstrated by comparing PALS-observed brightness temperatures with ODC-reconstructed postings. Fig. 2 shows a comparison of ODC-reconstructed brightness temperatures with observed L band horizontally polarized postings for July 2 and July 7, representing dry and wet conditions, respectively; related statistics are given in Table 1. The
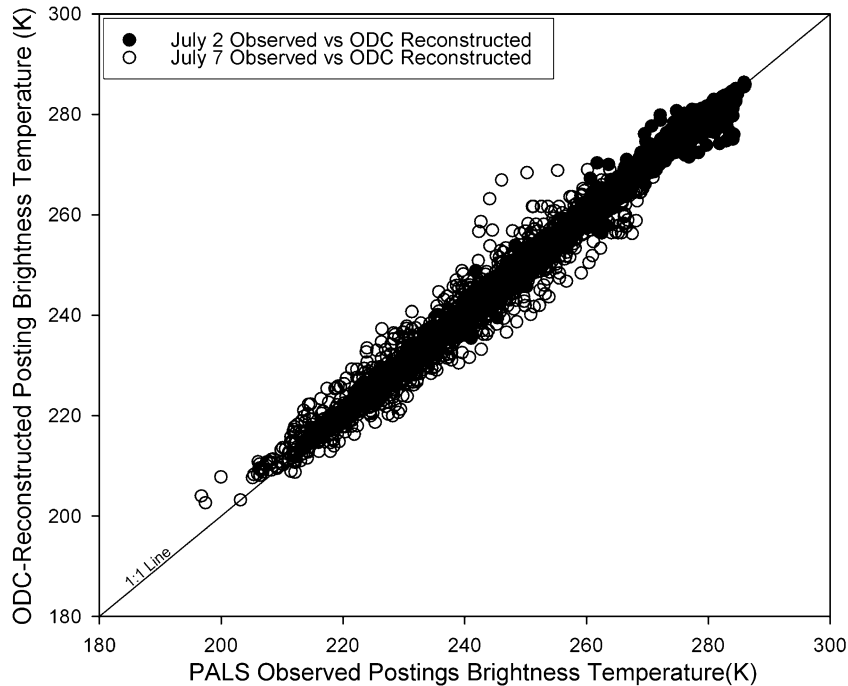
Fig. 2. Comparison of ODC-reconstructed posting L band H polarization brightness temperatures with PALS-observed TB for dry and wet conditions on July 2 and July 7, 2002, respectively.

mean absolute errors (MAE) for the 2 days are 0.51 and 1.19 K; the R^2 values are 0.97 for both days and the root mean square errors (RMSE) are 0.90 and 2.06 K, respectively. The means of the ODC-reconstructed brightness temperatures were not found to be statistically different from the postings.

4.2. Verification of ODC estimates

The ideal validation of ODC estimates would be with respect to independent TB observations. In the absence of such measurements, we defined a proxy with a subset of the PALS observations in which the Gaussian fraction is greater than 0.95. We refer to these observations as "pure" postings because over 95% of the contribution is from a single segment. A 'pure postings segment TB' is defined as the mean of all pure postings contained in the segment, the value of which is deemed to be the best estimate of the brightness temperature of that field. Such postings provide significant detail about the segment. However, in order to perform an independent verification of the ODC approach, we repeated the analysis with pure postings omitted, thereby isolating the pure postings subset for verification. The ODC-estimated segment TB (without the pure postings) for all of the days PALS was flown in July 2002 (dates: 1, 2, 5, 6, 7 and 8) are compared with pure posting segment TB in Fig. 3. Also shown in Fig. 3 are segment TB obtained by applying IDW interpolation to PALS observations. It is clear that the ODC results are in a better agreement with pure postings segment TB. The IDW smoothing can be noticed

in the overestimation at lower brightness temperatures (soybeans) and underestimation at higher values (corn). The associated statistics for corn and soybeans are shown in Table 2. Means, minima, maxima and variances for ODC and pure postings segment TB are similar, whereas IDW results in under- or overestimation of TB in higher or lower ranges, respectively. The means of ODC-estimated segment TB are statistically similar to the pure postings segment TB while that is not true for IDW-estimated segment TB. Mean absolute error (MAE) and root mean square error (RMSE) are significantly lower for ODC-estimated segment TB than for IDW-estimated segment TB.

Table 1
Statistics of observed and ODC-reconstructed postings for July 2 and July 7, 2002

|	Reconstructed postings, July 2	Observed postings, July 2	Reconstructed postings, July 7	Observed postings, July 7
Mean	276.40	276.40	244.05	243.99
Min	235.39	239.09	202.63	196.75
Max	286.34	286.03	273.40	273.58
Standard deviation	4.84	4.88	12.72	12.90
R^2	0.97		0.97	
MAE	0.51		1.19	
RMSE	0.90		2.06	
T-test w/ observed	Not a statistically significant difference		Not a statistically significant difference	
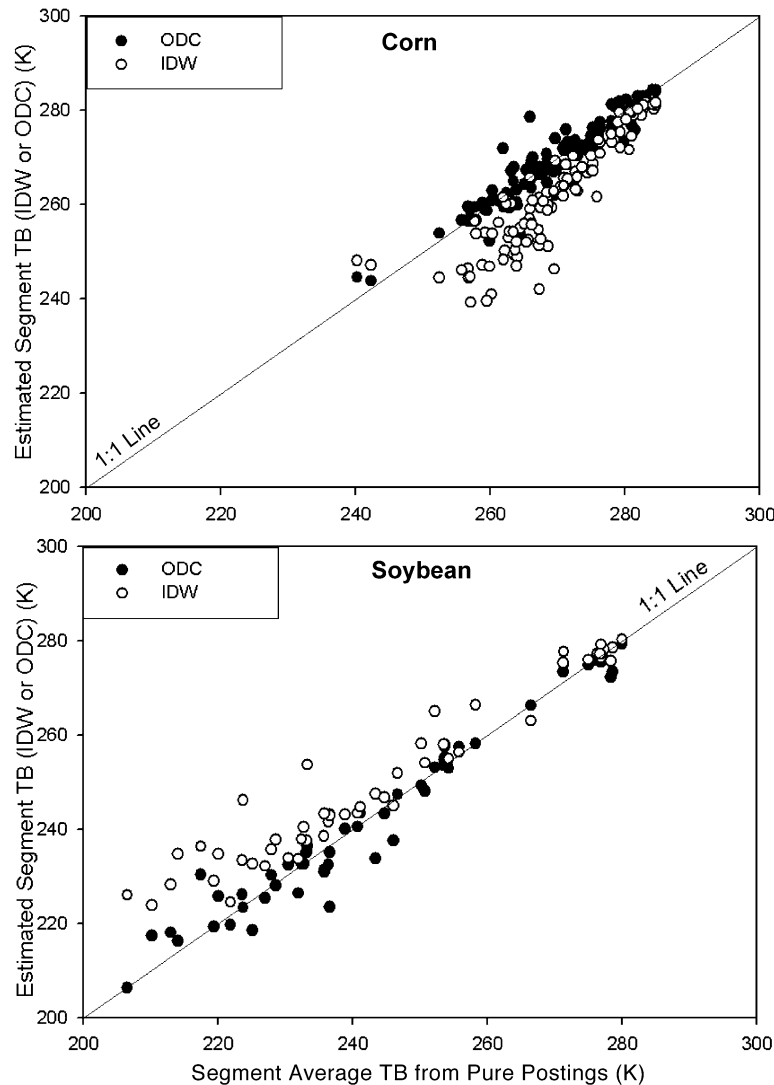
Fig. 3. Validation of ODC segment L band H polarization brightness temperatures, compared with segment averages derived from pure postings for all the days in July on which PALS was flown. In this application, the ODC analysis was performed with the pure postings omitted.

Pure postings represent a small portion of all postings, since they must be located near the center of a large segment. The other postings cover a heterogeneous mix of contributing segments within their footprints. To verify the efficacy of the technique over heterogeneous areas, randomly selected ODC-reconstructed postings were compared with the corresponding observed postings. This verification can be done only for the posting and not for the segments since a non-pure posting has contributions from more than one land cover type. One hundred observed postings were randomly omitted, one at a time, and the ODC analysis was performed. In this way, the verification data set is kept distinct from the analysis data set. The ODC-reconstructed posting estimates were then compared with the omitted observed postings. Fig. 4 shows the plot of ODC-reconstructed postings compared with the withheld observations for July 7. The observed omitted postings agree well with the ODC-reconstructed postings

with an R^2 of 0.98, an MAE of 1.32 K and an RMSE of 1.88 K (Table 3).

4.3. Comparison of ODC versus inverse distance weighted brightness temperature estimates

We illustrate the differences between the ODC and IDW brightness temperature estimates by plotting a transect corresponding to a part of a single flight line on July 7 (Fig. 5). The figure clearly illustrates the smoothing effect of interpolation that is particularly evident at land cover boundaries. The lower part of the figure shows PALS postings along with IDW- and ODC-estimated TB along the flight line. By definition, the PALS observations and IDW-interpolated estimates have identical values. The large difference between corn and soybean TB is obvious across the transect. The observed and IDW-interpolated TBs clearly illustrate the smoothing caused by the con-

Table 2
Comparison of corn and soybean ODC and IDW segment TB estimates with segment averages derived from 'pure' PALS postings on all days PALS was flown in July

	Pure	ODC w/o pure	IDW
Corn			
Mean	269.97	269.59	262.99
Min	240.20	243.88	239.27
Max	284.58	284.35	281.71
Standard deviation	8.92	9.00	11.81
R^2		0.88	0.78
MAE		2.25	7.21
RMSE		3.19	8.85
T-test w/ pure		Not a statistically significant difference	Statistically significant difference
Soybeans			
Mean	244.79	244.32	250.8
Min	206.52	206.38	223.88
Max	279.99	279.34	280.28
Standard deviation	21.22	20.76	17.46
R^2		0.96	0.86
MAE		2.71	6.29
RMSE		4.10	8.56
T-test w/ pure		Not a statistically significant difference	Statistically significant difference

tributions from neighboring land cover segments within the sensor footprint. In other words, the transition between crop types is more gradual in the observed and IDW-interpolated estimates. In contrast, ODC-estimated TBs preserve the sharp boundaries between different land cover types. Thus, the dynamic range of brightness temperatures between corn and soybeans is more pro-

nounced with the ODC estimates than with the IDW estimates.

The effect of smoothing by interpolation can also be seen clearly in Fig. 6, which shows a spatial comparison of IDW interpolated estimates with ODC. IDW-estimated TBs (panel D) are computed over the same 10 m grid that is used in the ODC analysis and averaged for each segment (panel C). Thus, the ODC-estimated segment TBs (panel B) in comparison with IDW-estimated segment mean TBs show that the IDW method yields a smaller difference between corn and soybeans (as seen in Fig. 5). The spatial structure of corn and soybean segments can also be deciphered in the ODC-estimated segment TB, whereas IDW grid or segment average interpolations are smooth and lack clarity.

Segment mean TB from corn and soybeans estimated in both the ODC and IDW methods are from statistically distinct populations. However, the separation in IDW estimates of corn and soybean TB during both dry and wet conditions is much smaller than that seen in ODC estimates. The improved ODC-estimated segment mean TB should potentially lead to better field scale soil moisture estimation. Evaluation of the improvement in soil moisture estimation involves treatment of retrieval algorithms, in situ data quality and sampling and data registration issues. This evaluation is important and is the subject of ongoing collaborative studies using the SMEX02 data.

5. Summary and discussion

The ODC technique uses the sensor antenna response function of a microwave remote sensor to deconvolve the
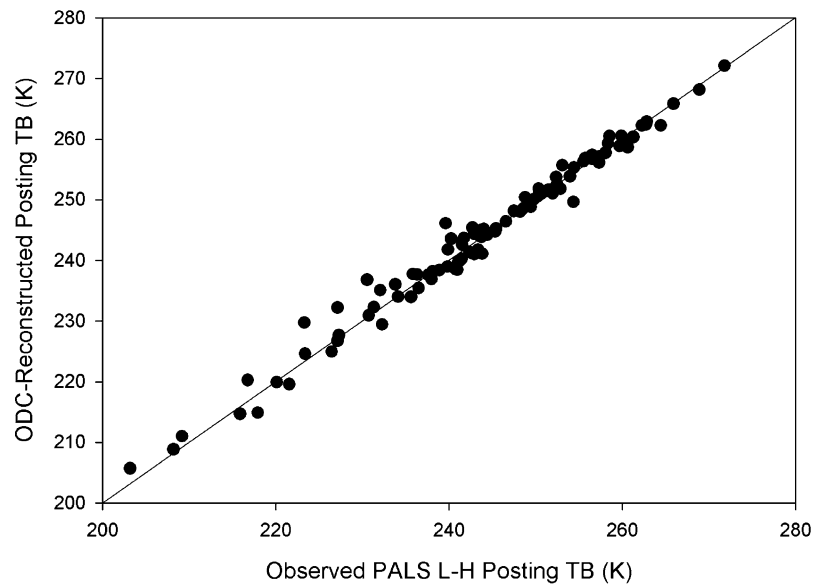

Fig. 4. Comparison of ODC-reconstructed brightness temperatures with omitted PALS postings for July 7, 2002.

Table 3
Statistics of ODC-reconstructed posting TB estimates with respect to observed PALS postings omitted in this ODC analysis for July 7, 2002

	ODC-reconstructed postings	Omitted observed postings
Mean	244.26	244.02
Min	205.67	203.20
Max	272.11	271.80
Standard deviation	13.53	13.84
R^2	0.98	
MAE	1.32	
RMSE	1.88	
T-test w/ Obs	Not a statistically significant difference	

observed brightness temperature into segment brightness temperatures. This technique can be applied to a regular grid or, as in this analysis, to an irregular land cover pattern of agricultural fields (segments). The technique was used to estimate field-scale brightness temperatures that we show to be more realistic and more accurate than conventional interpolation techniques in two ways. First, ODC-estimated TBs were shown to correlate better with PALS pure postings segment TB than with IDW-estimated segment TB. Pure postings were omitted from this analysis and used as the independent verification source. ODC estimated segment

TB were also shown to better characterize the dynamic range of brightness temperatures between corn and soybean fields, while interpolated TB unrealistically suppress the dynamic range between contrasting fields. Such increased fidelity in brightness temperature estimation may lead to improved field scale soil moisture retrieval.

Successful application of the ODC technique in this study can be attributed to observation over-sampling, large segments with relative homogeneity, and significant brightness temperature contrast among land cover components. The ODC technique can be of significant help in refining soil moisture retrieval algorithms compared to conventional interpolation methods that tend to smooth the transition between objects in a heterogeneous data field and suppress the overall dynamic range of the data. The ODC technique can also be effectively applied to other airborne microwave sensors supporting validation work in field experiments such as SMEX02.

Results of the analysis using only PALS L band horizontal polarization are presented in this paper. However, in addition to the L band horizontal polarization, we have also performed ODC analysis on L band vertical polarization. Brightness temperatures from vertical polarization show higher TB values, but the trends are similar. Likewise, similar conclusions can also be made from S band data.
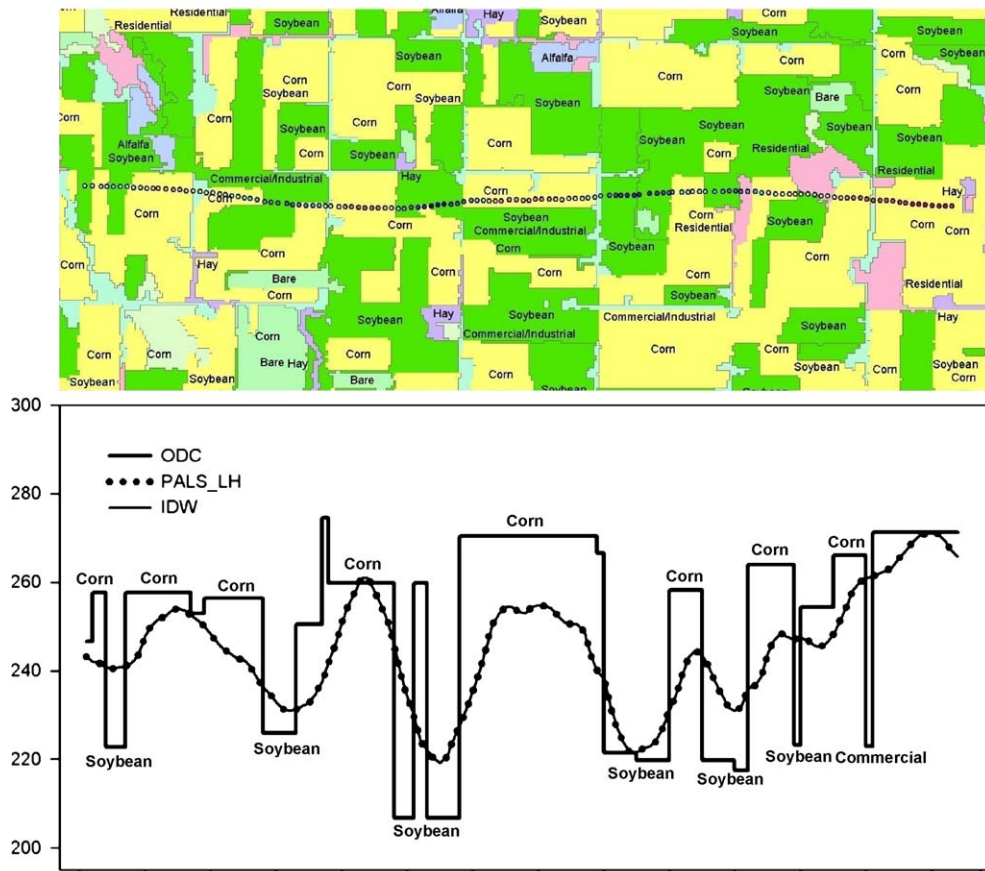

Fig. 5. Transect of PALS postings, land cover segmentation, IDW interpolation and underlying segment ODC brightness temperatures for July 7, 2002.
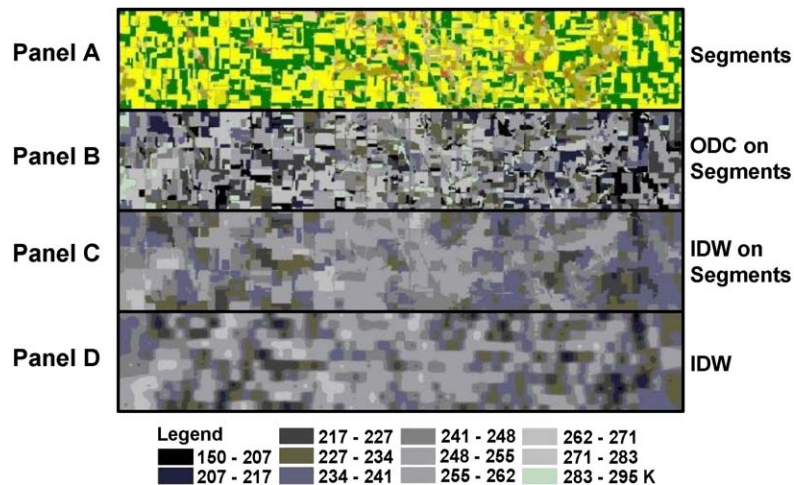
Fig. 6. ODC segment TB, IDW interpolated L band H polarization brightness temperatures averaged over each segment, and IDW estimates on a 10 m grid for the SMEX02 watershed study area on July 7, 2002. Yellow in the segments represent corn, whereas green in the segments represents soybeans.

Thus, the results from vertical polarization or the S band data are not presented for the sake of brevity.

Further research will examine the application of the ODC technique to space-based microwave sensors. It is possible that the application of the ODC technique is limited to conditions where the TB heterogeneity between grid cells (analogous to segments in this analysis) is greater than it is within each cell. ODC can be used to estimate TB for land surface areas on a regular grid as long as the grid cell dimension is greater than the mean distance between remote sensing observations (postings). This requirement leads to over-sampling of the cell by adjacent observations. With regards to the Advanced Microwave Scanning Radiometer for EOS (AMSR-E) on the Aqua satellite, the spacing between adjacent observations is 10 km whereas the AMSR-E IFOV extends approximately 75 km along track and 45 km across track. Therefore, ODC can be applied to AMSR-E on a 20–25 km grid, which is comparable to the 25 km EASE grid on which the AMSR-E brightness temperature and soil moisture products are currently averaged (using a method analogous to IDW in this analysis). Although results have not yet been evaluated, application of ODC to AMSR-E data may result in improvements over the current averaged TB reported for the EASE grid. It is likely that the application of the ODC technique to AMSR-E data will be useful to extend spatial coverage in the vicinity of shorelines of large water bodies. Near shorelines, the large sensor IFOV includes the water body with lower TB and the land area with typically higher TB. This renders useless any averaged observations within some distance of the coastline (roughly the dimension of the IFOV, or two to three IFOV depending on the accuracy required). This situation is analogous to the analysis presented in this paper where soybeans and corn vegetation biomass (and therefore microwave brightness temperatures) are significantly different. Thus, for a water body larger than the spacing between the observations, ODC can extract the shoreline with better clarity than the existing observations.

Acknowledgements

References

Anderson, M. C., Neale, C. M. U., Li, F., Norman, J. M., Kustas, W. P., Jayanthi, H., & Chavez, J. (2004). Upscaling ground observations of vegetation cover and water content during SMEX02 using aircraft and Landsat imagery. *Remote Sensing of Environment, 92*, 447–464 (this issue).

Cosh, M. H., Jackson, T. J., Bindlish, R., & Prueger, J. (2004). Watershed scale temporal persistence of soil moisture and its role in validating satellite estimates. *Remote Sensing of Environment, 92*, 427–435 (this issue).

Engman, E. T., & Chauhan, N. (1995). Status of microwave soil moisture measurements with remote sensing. *Remote Sensing of Environment, 51*, 189–198.

Jackson, T. J. (1993). Measuring surface soil moisture using passive microwave remote sensing. *Hydrological Processes, 7*, 139–152.

Jackson, T. J., & Schmugge, T. J. (1989). Passive microwave remote sensing system for soil moisture: Some supporting research. *IEEE Transactions on Geoscience and Remote Sensing, 27*, 225–235.

Jackson, T. J, LeVine, D. M., Swift, C. T., Schmugge, T. J., & Schiebe, F. R. (1995). Large area mapping of soil moisture using the ESTAR passive microwave radiometer in Washita '92. *Remote Sensing Reviews, 53*, 27–37.

Jackson, T. J., O'Neill, P. E., & Swift, C. T. (1997a). Passive microwave observation of diurnal surface soil moisture. *IEEE Transactions on Geoscience and Remote Sensing, 35*, 1210–1222.

Jackson, T. J., McNairn, H., Weltz, M. A., Brisco, B., & Brown, R. (1997b). First order surface roughness correction of active observations

for estimating soil moisture. *IEEE Transactions on Geoscience and Remote Sensing, 35,* 1065–1069.

Jackson, T. J., Le Vine, D. M., Hsu, A. Y., Oldak, A., Starks, P. J., Swift, C. T., Isham, J. D., & Haken, M. (1999). Soil moisture mapping at regional scales using microwave radiometry: The southern great plains hydrology experiment. *IEEE Transactions on Geoscience and Remote Sensing, 37,* 2136–2151.

Laymon, C. A., Belisle, W., Coleman, T., Crosson, W., Fahsi, A., Jackson, T., Manu, A., O'Neill, P., Senwo, Z., & Tsegaye, T. (1999). Huntsville '96: An experiment in ground-based microwave remote sensing of soil moisture. *International Journal of Remote Sensing, 20,* 823–828.

Laymon, C., Crosson, W., Jackson, T., Manu, A., & Tsegaye, T. (2001). Ground-based passive microwave remote sensing observations of soil moisture at S-band and L-band with insight into measurement accuracy. *IEEE Transactions on Geoscience and Remote Sensing, 39,* 1844–1858.

Long, D. G., & Daum, D. L. (1998). Spatial resolution enhancement of SSM/I data. *IEEE Transactions on Geoscience and Remote Sensing, 36,* 407–417.

Maidment, D. R. (1993). Handbook of hydrology. New York: McGraw-Hill.

Poe, G. (1990). Optimum interpolation of imaging microwave radiometer data. *IEEE Transactions on Geoscience and Remote Sensing, 28,* 800–810.

Ulaby, F. T., Moore, R. K., & Fung, A. K. (1986). Microwave remote sensing, active and passive. *From theory to applications, III.* Boston, MA: Artech House. pp. 1100.

Wilson, W. J., Yueh, S. H., Dinardo, S. J., Chazanoff, S. L., Kitiyakara, A., Li, F. K., & Rahmat-Samii, Y. (2001). Passive active L- and S-band (PALS) microwave sensor for ocean salinity and soil moisture measurements. *IEEE Transactions on Geoscience and Remote Sensing, 39,* 1039–1048.